Saccade direction encoding in the primate entorhinal cortex during visual exploration

Nathaniel J. Killian[a,b,c], Steve M. Potter[c], and Elizabeth A. Buffalo[b,d,e,f,1]

[a]Department of Neurosurgery, Massachusetts General Hospital, Boston, MA 02114; [b]Yerkes National Primate Research Center, Atlanta, GA 30329; [c]Laboratory for Neuroengineering, Wallace H. Coulter Department of Biomedical Engineering, Georgia Institute of Technology and Emory University School of Medicine, Atlanta, GA 30332; [d]Department of Neurology, Emory University School of Medicine, Atlanta, GA 30322; [e]Department of Physiology and Biophysics, University of Washington, Seattle, WA 98195; and [f]Washington National Primate Research Center, Seattle, WA 09195

Edited by Michael E. Goldberg, Columbia University College of Physicians, New York, NY, and approved October 29, 2015 (received for review September 3, 2014)

We recently demonstrated that position in visual space is represented by grid cells in the primate entorhinal cortex (EC), suggesting that visual exploration of complex scenes in primates may employ signaling mechanisms similar to those used during exploration of physical space via movement in rodents. Here, we describe a group of saccade direction (SD) cells that encode eye movement information in the monkey EC during free-viewing of complex images. Significant saccade direction encoding was found in 20% of the cells recorded in the posterior EC. SD cells were generally broadly tuned and two largely separate populations of SD cells encoded future and previous saccade direction. Some properties of these cells resemble those of head-direction cells in rodent EC, suggesting that the same neural circuitry may be capable of performing homologous spatial computations under different exploratory contexts.

vision | spatial representation | medial temporal lobe | head direction | grid cell

In visual exploration, the direction of saccadic eye movements carries important information about past and future gaze location. This information might be useful for optimal exploration of visual scenes and for memory processes that use information about spatial relationships. Encoding through ensembles of grid cells that represent gaze location (1) and saccade direction (SD) cells that represent gaze movement could provide the spatial information necessary to associate visual content with relative locations in visual space. Grid cells may provide location information, whereas SD cells may provide information about the relative ordering in space of viewed parts of the scene.

In rodents, head-direction cells have been defined as cells with an allocentric heading preference when the animal is within a particular environment (2). Identified first in the postsubiculum (3) and then in the thalamus (4, 5) and the entorhinal cortex (EC) (6), head-direction cells are considered an essential component of the rodent spatial navigation system. In primates, we are aware of one report of four head-direction cells identified in the macaque presubiculum (7) and two reports of activity in the human EC related to the direction of virtual movement (8, 9). Many studies have examined neuronal responses related to eye movement direction signals in head-fixed monkeys, most often with saccades to a limited number of locations (10, 11), and recently in more natural contexts (12). However, directional encoding has remained largely unexamined in primate medial temporal lobe structures, and the relationship between neuronal activity and saccade direction in the EC has not previously been examined in a free-viewing exploratory context. Because we recently identified spatial signals in the primate EC during visual exploration (i.e., visual border cells and grid cells), we reasoned that saccadic eye movement trajectories in primates might also be represented in the EC.

Results

Neurons were recorded from the posterior EC of two monkeys that were viewing images presented as part of a test of visual recognition memory (13, 14). During recordings, monkeys were allowed to move their eyes freely to explore complex visual images (Fig. 1*A*). The image sets had an approximately uniform distribution of salient content in the radial direction, reducing potential directional bias from the locations of salient features (Fig. S1). Previous analyses of these data identified grid cells that represent visual space in a consistent manner during the exploration of dynamic visual content (1). Here, we have performed additional analyses to describe changes in neuronal firing rate related to saccadic eye movements (Fig. 1*B*). Out of 193 neurons recorded in the posterior EC, there were 39 neurons (20.2%) that qualified as selective for saccade direction by passing the Rayleigh test for nonuniformity ($P < 0.05$). This represented a significant population of cells (binomial test, $P < 0.001$). Sixteen of these neurons showed directional selectivity in the presaccade period (future saccade cells), and 14 neurons were selective in the postsaccade period (previous saccade cells). Nine of the direction-selective neurons qualified as having a nonuniform saccade direction response in both pre- and postsaccade time periods. We will refer to these neurons collectively as SD cells, cells that demonstrated a significant nonuniform relationship between firing and the future or previous saccade direction (Fig. 2*A*). The laminar location of each recorded neuron was identified through current source density analysis and histology (*Materials and Methods*). SD cells were found in all layers of the EC, and SD cells often conjunctively encoded other types of information including grid-like spatial representations or representations of stimulus novelty (Fig. S2, Table S1, and *Materials and Methods*).

Significance

Characterizing the dynamic encoding of body orientation and eye movements in the brain is central to understanding spatial representation. Studies in rodents have revealed an allocentric heading representation system known as the head-direction network. Visual information is presumed to be critical to rodent head-direction encoding; however, differences in the primate and rodent visual systems along with differences in exploratory behaviors across species have made it difficult to directly extend the findings from rodents to primates. This study describes a previously unidentified functional cell type in the primate entorhinal cortex that shows selectivity for the direction of saccadic eye movements. Future research avenues critical to increasing our understanding of spatial representation in the brain are suggested.

Author contributions: N.J.K., S.M.P., and E.A.B. designed research; N.J.K. performed research; N.J.K. analyzed data; and N.J.K. and E.A.B. wrote the paper.

The authors declare no conflict of interest.

This article is a PNAS Direct Submission.

Freely available online through the PNAS open access option.

[1]To whom correspondence should be addressed. Email: ebuffalo@uw.edu.

This article contains supporting information online at www.pnas.org/lookup/suppl/doi:10.1073/pnas.1417059112/-/DCSupplemental.

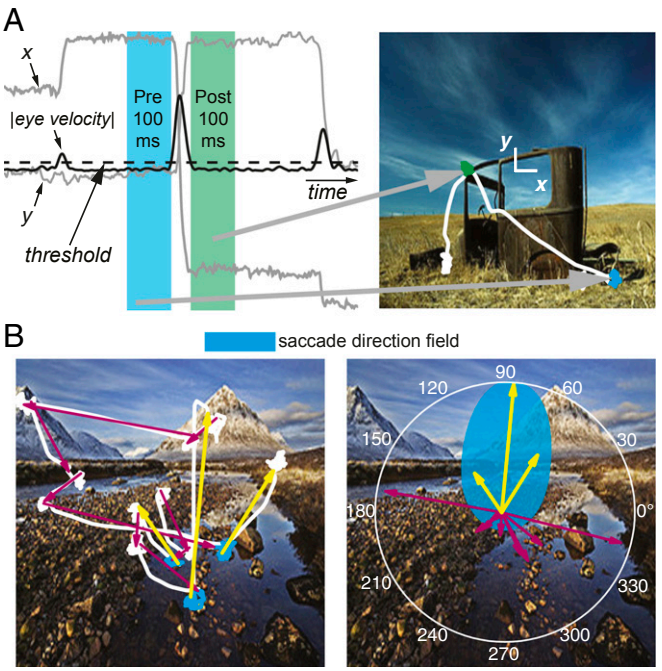

Fig. 1. Overview of saccade direction analysis. (*A*) For each cell, the firing rate 100 ms before the magnitude of the eye velocity crossed the saccade detection threshold (25°/s, dashed line) and the firing rate 100 ms after the eye velocity magnitude went below threshold were compared with the angle of saccades. This comparison was made using all saccades in each session with at least 100 ms of fixation before and after the saccade. (*B*) A hypothetical SD cell with the preferred saccade direction shown in cyan would have increased firing before the saccades depicted with yellow arrows but not before the saccades represented by magenta arrows. For direction analyses, saccades were treated as if they had started at the origin (*Right*). The white curves plotted on top of the photographs in *A* and *B* represent gaze location.

The direction corresponding to the peak firing rate was considered to be the "preferred direction." The preferred directions of SD cells are plotted in Fig. 2*B*. Overall, the preferred directions tended to be in the upper hemifield (mean direction of 96°, $P < 0.05$; Rayleigh test). The origin of this effect is not clear and may be attributable to sampling clusters of cells with similar preferred directions. The width of tuning was taken to be the circular variance, a value ranging from 0 for tuning at a single direction to 1 for a uniform circular distribution. Directional tuning was relatively broad, with a median circular variance of 0.81 (Fig. 2*C*). Tuning width increased with distance from the rhinal sulcus ($\rho = 0.56$, $P < 0.001$, $n = 39$; Spearman's rank correlation) but not with distance from the posterior EC border ($\rho = 0.15$, $P = 0.37$, $n = 39$; Spearman's rank correlation) (Fig. 2*D* and Fig. S3). This tuning correlation is similar to the anatomical gradient observed in grid cell spacing (1, 6, 15) and is consistent with the recently described increase in the tuning width of head-direction cells along the dorsoventral axis in rodents (16). Thus, colocalized visual grid cells and SD cells demonstrate similar anatomical gradients with respect to the scale of the spatial representation.

The time courses of the modulations in firing rates of SD cells are shown in Fig. 3*A*. The firing rates for the future saccade group were significantly higher in the preferred direction compared with the anti-preferred direction in the presaccade time period for the shaded time region identified (−66 to 24 ms, $P < 0.05$; cluster-based nonparametric permutation test). Similarly, for the previous saccade group, firing rates were higher after saccades were initiated in the preferred direction (−19 to 87 ms, $P < 0.05$). Considering the average normalized firing rate, the peak firing rate for the future saccade group occurred at 29 ms before saccade onset, and the peak firing rate for the previous saccade group occurred at 14 ms after saccade onset. The distributions of peak firing-rate latencies in the preferred direction, considering all cells individually, are shown in Fig. 3*B*. Although there was some variability in the timing of the peak rate for individual cells, the future and previous SD cells tended to demonstrate peak firing in the period before or after the saccade start, respectively.

We next examined whether saccade direction could be predicted from the activity of ensembles of simultaneously recorded SD cells. A circular–linear regression was performed for each group of simultaneously recorded SD cells (17). The resulting regression model (*Materials and Methods*) was used to predict saccade direction based on SD cell ensemble firing rates. Predicted saccade direction was positively correlated with actual saccade direction (Fig. 4). The prediction improved for larger neuronal ensembles ($\rho = 0.80$, $P < 0.01$; Spearman's rank correlation), which is expected for groups of simultaneously recorded neurons with firing that is not highly correlated. The ability to decode a range of directions from firing rate supports the idea that populations of SD cells in the EC encode eye movement trajectories. Trajectory information may assist in exploring complex visual scenes and aid memory formation by permitting the proper grouping of visual information at discrete locations in the visual field.

Discussion

Here, we have identified neurons in the primate EC that are preferentially active around the time of eye movements made in a preferred direction. This response property may be inherited via projections from structures that encode saccade direction or have preferred direction axes related to eye movement or eye position. Candidate structures include the parietal cortex (18) and thalamic nuclei such as the lateral dorsal nucleus of the thalamus (LD) (19). LD neurons encode eye position along preferred direction axes in macaques, with the firing rate tending to increase before saccades are made into the preferred direction and then maintaining activity during fixation (19). LD has reciprocal connections with posterior EC (20, 21) and also projects densely to the presubiculum (22, 23). The inferior parietal lobule (IPL), which contains cells with saccade-related activity, projects densely to the presubiculum and lightly to posterior EC (24, 25). The presubiculum is known to send a massive projection to posterior EC (24). In view of these anatomical connections and the functional properties of neurons in LD and the IPL, information about eye position or saccades along preferred directions could reach posterior EC through direct input from LD and the IPL and indirectly through input from the presubiculum.

Comparing the firing properties of SD cells to other cells that encode eye movements may provide some clues to their function. Cells that encode corollary discharge signals and their target neurons, such as the medial dorsal nucleus of the thalamus and the frontal eye fields, tend to have maximal rates near the onset of or shortly after the eye movement (26). Accordingly, the timing of the firing-rate modulation in some SD cells is consistent with a corollary discharge signal. The firing of future saccade SD cells peaked as early as 68 ms before the saccade movement, indicating that some SD cells could be involved in the early stages of movement planning or the directing of attention to stimulus features outside of the central fixation region. Future studies involving activation and inactivation of regions that encode eye movements, similar to experiments performed to identify corollary discharges (27), will likely be necessary to determine which eye movement signals identified in the EC represent planning, attention, corollary discharges of movement commands, or eye position.

We note that because the animals were head-fixed and seated in the same location for each experiment, we are not able to determine whether SD cells encode information in retinocentric, head-centric, body-centric, or allocentric coordinates. Head-direction cells in the rodent EC appear to encode allocentric head

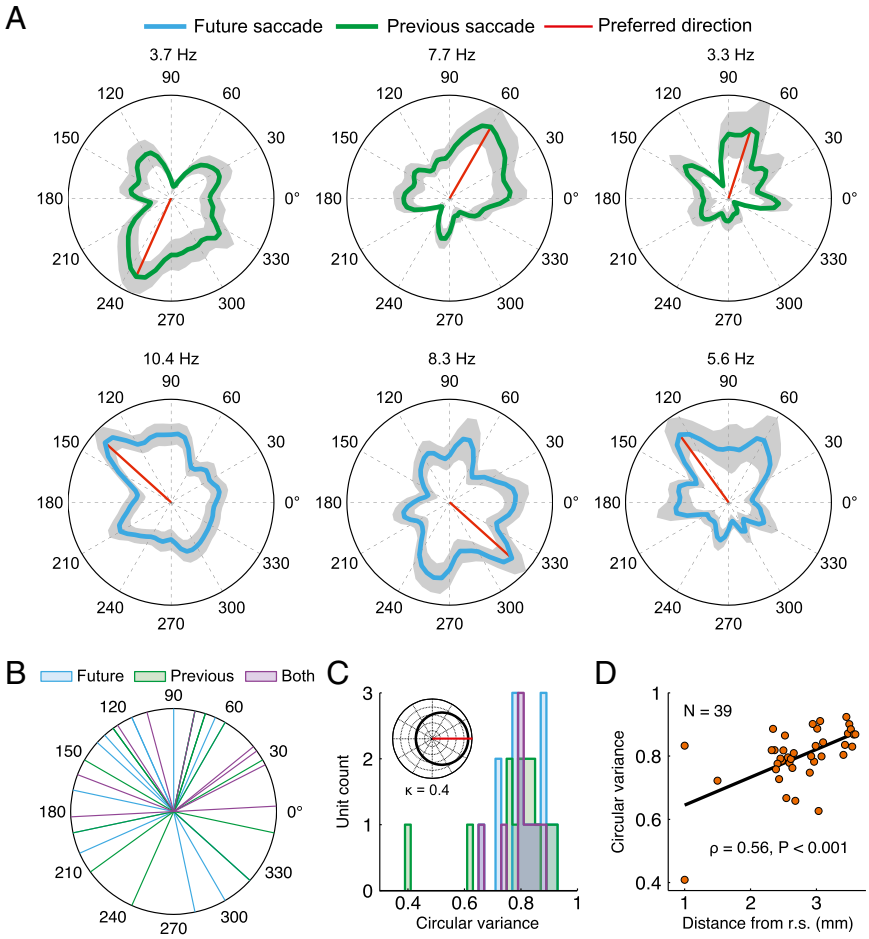

Fig. 2. SD cell firing properties. (*A*) Angular probability densities representing perisaccade firing rates for six example cells with significantly nonuniform firing-rate distributions (Rayleigh test, $P < 0.05$). Plots in the upper row depict cells with significant previous saccade distributions, and plots in the lower row depict cells with a significant future saccade distribution. The maximum firing rate is listed at the top of each plot. The shaded regions represent the density ± 1 standard deviation. (*B*) Distribution of preferred directions (cyan: future saccade cells, $n = 16$; green: previous saccade cells, $n = 14$; purple: both future and previous, $n = 9$). (*C*) Histogram of the variance of tuning. The median variance was 0.81 across groups (similar to a von Mises distribution with $\kappa = 0.4$; *Inset*). (*D*) The width of tuning of individual neurons to a preferred saccade direction increased with distance from the rhinal sulcus (r.s.), as shown in the plot of circular variance for all SD cells. The black line is the best-fit line.

direction independent of body location or movement, i.e., the classic compass-like head-direction signal observed in many other regions (2, 6, 7, 28). One interpretation of this compass-like firing is that head-direction cells in the EC represent attention to some visual region along a characteristic preferred direction, which is compatible with the present results. However, we do not know whether SD cells would encode allocentric head orientation in a behavioral situation analogous to the rodent foraging paradigm because we have not examined the same primate EC neurons during both locomotion and eye movements. Likewise, we are not aware of any studies in rodents that have simultaneously examined EC responses during eye movements and locomotion.

It is interesting to consider whether the differences between rodent and primate vision could help to explain the apparent disparity between encoding of head orientation in rodent EC and encoding of eye movements in primate EC. The primate visual system is distinctly different from the visual system of common laboratory rodents, which have a larger field of view, make few saccades, and lack a specialized retinal region like the primate fovea (29–32). Consequently, sampling by moving the visual field via head movements in rodents might be similar to moving the fovea with the eyes in primates. Furthermore, it is possible that the neural circuitry involved in representing head direction in rodents may have evolved to represent saccade direction in primates. In support of this idea, the lateral dorsal nucleus of the thalamus, which encodes head direction and is important for place-field representation in rodents (33, 34), appears to encode eye position in macaques, as previously described (19). Similarly, it has recently been demonstrated that the nucleus prepositus, thought to be an important part of the rodent head-direction network (2), predominantly outputs eye movement-related information in primates (35). The present data, with the identification of SD cells, provide evidence that this analogous neural circuitry may extend to the entorhinal cortex. Future studies in both rodent and primate models will be needed to determine whether the same neural circuits perform homologous computations or whether independent circuits are recruited for processing movements of different types.

Considering how SD cells might interact with other neurons, SD cells and neurons that provide directional signals in the primate hippocampal formation (7, 8) could form the basis of more complex spatial representations (1, 36) through local connections (37). For example, access to fixation location information in advance of gaze actually reaching the location could help prepare visual grid cells to fire in alignment with their respective firing fields. In conjunction with neurons that encode

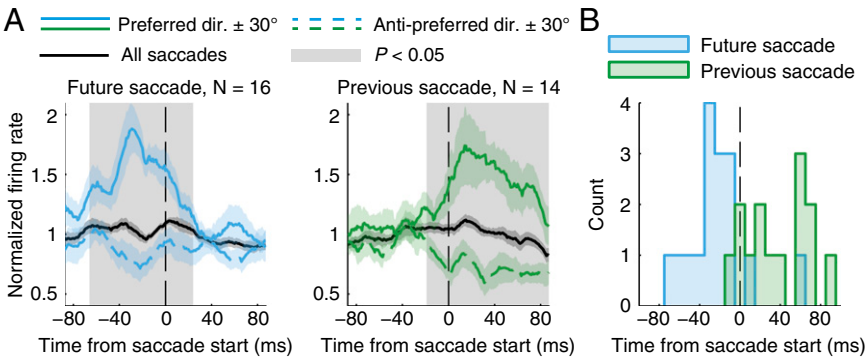

Fig. 3. Time course of saccade direction encoding. (*A*) The firing rate normalized to the average rate over all saccades is shown for the 16 cells that encoded only future saccade direction and 14 cells that encoded only previous saccade direction. Rates are shown for all saccades (black), the preferred direction ± 30° (solid lines), and the anti-preferred direction ± 30° (dashed lines). Curves represent means ± SEM, and the gray shading represents a time region of significant difference between the preferred and anti-preferred directions ($P < 0.05$). (*B*) Histogram of peak firing latencies (10-ms bin width). The median latency was −27 ms for future saccade cells and +38 ms for previous saccade cells (same groups as in *A*).

information about specific items (38), these neuronal signals may then be temporally matched to aid in forming associations between items and the places where the items were encountered.

It is possible that grid cells and SD cells might provide the necessary ingredients to support visual path integration in primates. However, it is important to note that primates and rodents may differ in terms of path integration ability as well as which brain structures are critical for this ability. A recent study demonstrated that, in humans, damage to medial temporal lobe structures including the entorhinal cortex does not impair path integration, unlike in rats (39). By contrast, those same patients with medial temporal lobe damage demonstrated significant impairment in the formation of new memories. These findings suggest that neural signals in the primate entorhinal cortex, including grid and saccade direction signals, may not be critical for path integration and may instead play a role in providing spatial structure for memory formation. This contrasts with the rodent model of spatial representation in the hippocampal formation that is based on continuous self-motion information (40). Taken together with the present results, these data suggest that the EC in different species may be suited to perform similar computations independent of the sensory modalities used and independent of the functional significance of these computations [i.e., path integration vs. spatial structuring (41)].

Materials and Methods

Spikes were recorded from posterior EC neurons of two adult male rhesus macaques with a laminar electrode array. The monkeys performed the Visual Preferential Looking Task (VPLT) (1, 14) as their gaze was tracked with an infrared camera. Saccades were detected during image viewing trials by thresholding eye movement speed. Relationships between firing rate and angular saccade direction were then assessed with circular statistics. All experiments were carried out in accordance with protocols approved by the Emory University Institutional Animal Care and Use Committee.

Behavioral Task. The animals performed the VPLT, which was the same as in our previously published work (1, 14, 42, 43). Briefly, a novel set of 200 complex visual images was chosen for each session, and each image was viewed twice while eye position was tracked with an infrared camera (ISCAN). An initial 1-s fixation period preceded each viewing. The images subtended an 11° × 11° region of a cathode ray tube monitor (120-Hz refresh rate) and were viewed until the gaze exited the image region or until the viewing time limit was reached (7 s for animal TT; 5 s for animal MP). One experiment was performed in animal MP with 33° × 25° images that were viewed for a cumulative 10 s. The animals were head-fixed, and the location of the animal and the monitor (60 cm) was the same for each session.

Electrophysiology. We recorded spiking activity (250–8,000 Hz) from posterior EC neurons in two adult male rhesus macaques with the use of a laminar electrode array mounted on a tungsten microelectrode (12-site, 30-μm diameter, 150-μm spacing; FHC). We recorded 193 single units from the posterior region of the EC (up to interaural +16) of 2 monkeys (MP and TT). Recordings were performed using hardware and software from Plexon, and all subsequent analyses were performed using custom software and the CircStat toolbox (44) in the MATLAB environment (MathWorks). All recordings were performed in the left hemisphere. Recording sites were planned with the aid of a stereotaxic atlas (45) and structural magnetic resonance images obtained after chamber implantation using both extra- and intracranial fiducial markers. The recording chamber center was located in three dimensions to within 1 mm using 0.5 × 0.5 × 1.0 mm voxels. The electrode array was placed in a polyimide-lined stainless steel guide tube and was slowly lowered through a craniotomy at the beginning of each recording session. Custom 3D-printed guide tube support structures and the high stiffness of the array ensured the straight trajectories that were necessary for the long

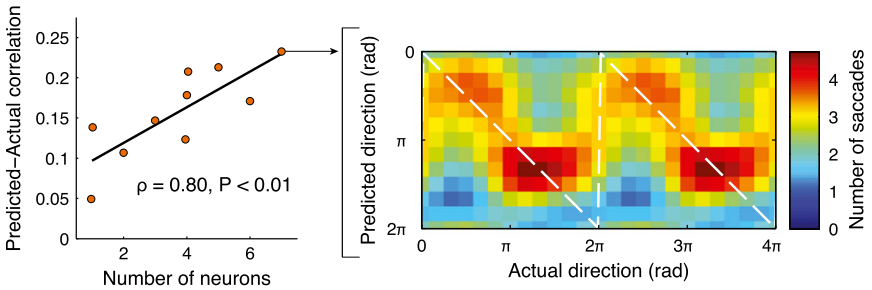

Fig. 4. SD cells may encode viewing paths. (*Left*) Taking all recorded ensembles ($n = 10$), prediction accuracy (the predicted–actual direction circular correlation coefficient) improved as the number of neurons in the ensemble increased. The best-fit line is in black. (*Right*) Predicted saccade direction is plotted against actual saccade direction in this histogram for an ensemble of seven neurons (391 saccades). Warmer colors represent a greater number of saccades, and the white dashed line corresponds to exact prediction. Two cycles are shown for clarity.

dorsal–ventral penetrations. The array was advanced out of the guide tube to the recording site while the monkeys performed unrelated tasks. Recordings were initiated after stable spiking could be verified (usually about 30 min). Spikes were sorted offline into distinct clusters using principal component analysis (Offline Sorter; Plexon). Sorted clusters were classified as single units if the root-mean-square error of the waveforms from the mean waveform was below 0.3 after normalizing to the mean waveform of the cluster, which was empirically found to help restrict waveform groups to signals from single neurons. In addition, units with fewer than 150 spikes and less than 500 s of total sampling were excluded from the analyses to reduce sampling error.

Layer Classification. Location within the EC was classified with the aid of current source density (CSD) profiles obtained from simultaneously recorded local field potentials (46). CSD curves were aligned to a template CSD profile obtained from one monkey using electrolesioning followed by histology. A stereotypical phase reversal in the CSD was seen near layer II when averaging the CSD aligned to saccade onset. This phase reversal was used to estimate the border between layers II and III. Layer III was then estimated as occupying the next 5 recording sites, based on the approximate thickness of layer III. Recordings from sites dorsal to the estimated layer III were then considered to be in deep layers (layers V/VI).

Saccade Direction Analyses. Saccades were defined through an eye movement speed-thresholding procedure. To reduce detection of saccades attributable to noise in the recorded eye position, thresholding was performed after filtering the gaze location with a 30th-order low-pass (30-Hz cutoff) linear phase digital finite impulse-response filter. Saccades were detected by thresholding the filtered eye movement speed at 25°/s. A saccade was defined by a pair of rising and falling threshold crossings. The corresponding saccade direction was defined as the angle of displacement from the first to the last sample of the saccade.

Time periods of 100 ms before and after saccades were used to characterize neuronal firing related to saccade direction. The final saccades away from the image were not included in saccade direction analyses because of the requirement of 100 ms of fixation within the image region before and after the saccade. Any saccades with flanking periods shorter than 100 ms were removed from the analysis. Next, to reduce bias from any stimulus factors that may not have been uniformly distributed when sampled by saccadic eye movements, we pseudorandomly down-sampled the saccade events such that the same saccade count was present in each quadrant. After this procedure, no session had a nonuniform saccade direction distribution (Rayleigh test, $P > 0.05$ for all sessions). Firing-rate distributions were estimated using a kernel density-estimation procedure (Gaussian kernel, 9° standard deviation). Spike count densities were normalized by saccade densities, yielding firing rate as a function of saccade direction (Fig. 2*A*). The standard deviations of the densities were estimated using bootstrap resampling (1,000 resamples for each cell). The Rayleigh test was performed on the firing-rate densities to test for nonuniformity in the firing rate–saccade direction relationship (47). SD cells were preliminarily identified as those cells passing the Rayleigh test ($P < 0.05$) in the 100 ms preceding a saccade or 100 ms after the end of a saccade when considering the saccades as defined above. The Rayleigh test assumes that samples are drawn from a unimodal von Mises distribution. The probability density function of the von Mises distribution, f, for angle θ with mean and concentration parameters μ and κ is given by

$$f(\theta|\mu,\kappa) = \frac{e^{\kappa\cos(\theta-\mu)}}{2\pi I_0(\kappa)},$$

where $I_0(\kappa)$ is the modified Bessel function of the first kind of order zero. Kuiper's test was used to compare the firing-rate distribution to a von Mises distribution, with mean and concentration parameters estimated from the observations, for each cell. Kuiper's test indicated that only one of the cells identified as an SD cell significantly deviated from a von Mises distribution, and this cell was removed from further analyses.

The tuning curves often exhibited multiple peaks rather than being smooth curves with only a single peak. A unimodal von Mises distribution was not rejected with Kuiper's test, meaning the deviations from a unimodal von Mises were not found to be statistically significant. Nevertheless, because it is possible that a statistical model including additional parameters could provide better fits to the tuning curves, we sought to identify the best statistical model by examining the extent to which tuning curves could be described by a weighted combination of von Mises distributions. For each cell, we estimated parameters for a single von Mises distribution and for an additive mixture of two or three von Mises distributions with a finite mixture distribution p given by

$$p(\theta) = \sum_{i=1}^{N} w_i f_i(\theta),$$

with component von Mises probability density functions $f_i(\theta)$ as defined above and with N equal to the number of mixture components ($w_1 = 1$ when $N = 1$). Maximum-likelihood estimation (MLE) was used to fit the mean and concentration parameters for the superposed distributions as well as the weights, w_i, for each distribution i in the mixture (each weight was constrained to be between 0 and 1, with all weights summing to 1). The MLE was performed by numerically maximizing the log-likelihood for each mixture model, resulting in a maximum value $\hat{L}$. The Bayesian information criterion (BIC) was then computed for each mixture. The BIC is given by

$$\mathrm{BIC} = -2\hat{L} + k\ln n,$$

where k is the number of free parameters in the mixture model, and n is the number of saccade events sampled. In MLE, additional parameters can increase the likelihood, but the BIC introduces a penalty for the addition of parameters such that the model with the lowest BIC can be considered to be the best or most efficient model in the set of models being compared. Most SD cells (39 of 42) had the lowest BIC with one von Mises distribution; three had the lowest BIC with two von Mises distributions. The latter three cells had bimodal tuning curves and were thus eliminated from further analyses because we defined SD cells as having unimodal firing-rate distributions. Depictions of the mixture models are presented in Fig. S4.

To avoid erroneously identifying SD cells because of stimulus or behavioral biases, we removed cells with significant border scores or significant linear firing-rate correlations with saccade amplitude or stimulus properties of salience, brightness, brightness contrast, color contrast, or color at the pre- or postsaccade fixation locations when there was a corresponding overall bias in the session for the given factor (Pearson product–moment correlation coefficient, $P < 0.05$). In general, it is possible for firing fields covering some region(s) of visual space to modulate firing rate. The occurrence of conjunctive SD and grid cells (Fig. S2) demonstrates that gaze location does modulate firing of some SD cells. View field(s) potentially confound the analysis of saccade direction if there is not a uniform distribution of saccades into or out of any such regions. To address this issue, we computed the spatial information rate (48) on firing-rate maps for each cell after taking the selection of saccade occurrences within ±30° of the preferred direction and compared this to a permutation distribution of 100 shuffled rate maps (rate map values were pseudorandomly assigned to new locations for each shuffling). Only 1 of 39 cells was found to have a significant spatial information rate ($P < 0.05$), which does not deviate from the number expected by chance with $\alpha = 0.05$. Thus, we did not detect a statistically significant bias from gaze location in the population of SD cells.

Firing-rate time courses were computed with a sliding 25-ms Gaussian window (12.5-ms standard deviation), and the peak latency was defined by the time of the maximum value in the average rate curves. The temporal regions of significant differences between preferred and anti-preferred directions in Fig. 3 were computed using a cluster-based nonparametric permutation test ($P_{\text{two-sided}} < 0.05$; 15,000 randomizations; $P < 0.1$ cluster threshold using a dependent-samples t test for each randomization) (49).

A circular–linear regression model was used to predict saccade direction based on firing rate (17). The predicted saccade angle, θ, is related to the ensemble vector of firing rate, x, via estimated parameters μ and β:

$$\theta = \mu + 2\tan^{-1}(\beta \mathrm{x}).$$

Saccade occurrences with correspondingly low firing rates were excluded: to be included in the model-fitting procedure, only occurrences in which the firing rate of at least one unit in the ensemble exceeded 0.4–2 times its mean rate (this threshold value was automatically optimized for each ensemble). To avoid overfitting, only ensembles with at least 100 saccade occurrences passing the rate threshold were used. The resulting samples had 278 ± 135 (mean ± standard deviation; $n = 10$ ensembles) saccade occurrences per ensemble. Both pre- and postsaccade firing rates were included in the model for units belonging to both future and previous saccade SD cell groups.

Additional Firing-Rate Analyses. Data from the image-presentation periods were concatenated across trials. Spikes and eye position sampled at 1 kHz were binned into square bins over the viewing region. Rate maps were then computed by applying a Gaussian-smoothing procedure to these histograms (50). Spatial autocorrelations were computed to calculate the gridness score. The spike train was shifted in 100 linearly spaced increments from 20 s into the session to the end of the session minus 20 s, and the resulting rate maps, spatial autocorrelations, and gridness scores were calculated. Units with a

gridness score above the 95th percentile of the surrogate data for each unit were considered grid cells. See ref. 1 for additional details.

Cells with a border score above the 95th percentile for 100 time-shifted permutations (the same permutations used for gridness scores) were classified as significantly preferring to fire along borders. Any SD cells with a significant border score were removed from analyses because of the potential saccade direction bias at image borders (i.e., SD cells could appear to be border cells and vice versa). The border score was the same as that used by Solstad et al. (51); however, where Solstad et al. used a rate map threshold of 30% of the maximum rate and a border score cutoff of 0.5, we used a rate map threshold equal to the mean firing rate over all bins and a permutation distribution to define significant border scores. Significant border scores ranged from 0.53 to 0.69. The border score, b, was calculated by comparing the maximum coverage of a given stimulus edge by a single firing field, c_M, to the firing rate-weighted average distance to the nearest edge, d_m:

$$b = \frac{c_M - d_m}{c_M + d_m}.$$

On average, the EC units exhibited a match suppression effect as reported previously (38). As a population, the EC units exhibited a decreased firing rate for the repeated stimulus from about 250 to 500 ms after stimulus onset. To analyze the firing rates for individual units, spike counts from 250 to 500 ms after stimulus onset were compared with a Student's *t* test to spike counts 500 to 250 ms before stimulus onset. Variable trial lengths were allowed, and only trials that lasted at least 310 ms were included in the analysis. Units were classified as visually responsive if either the encoding (novel stimulus presentation) or recognition (repeated stimulus presentation) trials had a significant difference in firing rate during viewing compared to the prestimulus time period. Of the visually responsive units, units with memory responses were identified using a Student's *t* test to compare the same time windows after stimulus onset with paired novel and repeat trials.

ACKNOWLEDGMENTS. The authors thank M. L. Jutras and K. Staikov for assistance with experiments; M. J. Jutras, D. Solyst, and M. Meister for helpful discussion; and S. Koenig for assistance with the analysis of image salience. Funding for this work was provided by National Institute of Mental Health Grants MH080007 (to E.A.B.) and MH093807 (to E.A.B.) and National Center for Research Resources Grant P51RR165 (currently Office of Research Infrastructure Programs/Office of the Director Grant P51OD11132).

1. Killian NJ, Jutras MJ, Buffalo EA (2012) A map of visual space in the primate entorhinal cortex. *Nature* 491(7426):761–764.
2. Taube JS (2007) The head direction signal: Origins and sensory-motor integration. *Annu Rev Neurosci* 30:181–207.
3. Taube JS, Muller RU, Ranck JB, Jr (1990) Head-direction cells recorded from the postsubiculum in freely moving rats. I. Description and quantitative analysis. *J Neurosci* 10(2): 420–435.
4. Taube JS (1995) Head direction cells recorded in the anterior thalamic nuclei of freely moving rats. *J Neurosci* 15(1 Pt 1):70–86.
5. Muller RU, Ranck JB, Jr, Taube JS (1996) Head direction cells: Properties and functional significance. *Curr Opin Neurobiol* 6(2):196–206.
6. Sargolini F, et al. (2006) Conjunctive representation of position, direction, and velocity in entorhinal cortex. *Science* 312(5774):758–762.
7. Robertson RG, Rolls ET, Georges-François P, Panzeri S (1999) Head direction cells in the primate pre-subiculum. *Hippocampus* 9(3):206–219.
8. Jacobs J, Kahana MJ, Ekstrom AD, Mollison MV, Fried I (2010) A sense of direction in human entorhinal cortex. *Proc Natl Acad Sci USA* 107(14):6487–6492.
9. Doeller CF, Barry C, Burgess N (2010) Evidence for grid cells in a human memory network. *Nature* 463(7281):657–661.
10. Barash S, Bracewell RM, Fogassi L, Gnadt JW, Andersen RA (1991) Saccade-related activity in the lateral intraparietal area. I. Temporal properties; comparison with area 7a. *J Neurophysiol* 66(3):1095–1108.
11. Munoz DP, Wurtz RH (1995) Saccade-related activity in monkey superior colliculus. I. Characteristics of burst and buildup cells. *J Neurophysiol* 73(6):2313–2333.
12. Fernandes HL, Stevenson IH, Phillips AN, Segraves MA, Kording KP (2014) Saliency and saccade encoding in the frontal eye field during natural scene search. *Cereb Cortex* 24(12):3232–3245.
13. Manns JR, Stark CE, Squire LR (2000) The visual paired-comparison task as a measure of declarative memory. *Proc Natl Acad Sci USA* 97(22):12375–12379.
14. Jutras MJ, Buffalo EA (2010) Recognition memory signals in the macaque hippocampus. *Proc Natl Acad Sci USA* 107(1):401–406.
15. Yartsev MM, Witter MP, Ulanovsky N (2011) Grid cells without theta oscillations in the entorhinal cortex of bats. *Nature* 479(7371):103–107.
16. Giocomo LM, et al. (2014) Topography of head direction cells in medial entorhinal cortex. *Curr Biol* 24(3):252–262.
17. Fisher NI, Lee AJ (1992) Regression models for an angular response. *Biometrics* 48(3): 665–677.
18. Colby CL, Goldberg ME (1999) Space and attention in parietal cortex. *Annu Rev Neurosci* 22:319–349.
19. Schlag-Rey M, Schlag J (1984) Visuomotor functions of central thalamus in monkey. I. Unit activity related to spontaneous eye movements. *J Neurophysiol* 51(6):1149–1174.
20. Insausti R, Amaral DG, Cowan WM (1987) The entorhinal cortex of the monkey: III. Subcortical afferents. *J Comp Neurol* 264(3):396–408.
21. Saunders RC, Mishkin M, Aggleton JP (2005) Projections from the entorhinal cortex, perirhinal cortex, presubiculum, and parasubiculum to the medial thalamus in macaque monkeys: identifying different pathways using disconnection techniques. *Exp Brain Res* 167(1):1–16.
22. Amaral DG, Cowan WM (1980) Subcortical afferents to the hippocampal formation in the monkey. *J Comp Neurol* 189(4):573–591.
23. Robertson RT, Kaitz SS (1981) Thalamic connections with limbic cortex. I. Thalamocortical projections. *J Comp Neurol* 195(3):501–525.
24. Insausti R, Amaral DG (2008) Entorhinal cortex of the monkey: IV. Topographical and laminar organization of cortical afferents. *J Comp Neurol* 509(6):608–641.
25. Ding SL, Van Hoesen G, Rockland KS (2000) Inferior parietal lobule projections to the presubiculum and neighboring ventromedial temporal cortical areas. *J Comp Neurol* 425(4):510–530.
26. Sommer MA, Wurtz RH (2002) A pathway in primate brain for internal monitoring of movements. *Science* 296(5572):1480–1482.
27. Wurtz RH, Sommer MA (2004) Identifying corollary discharges for movement in the primate brain. *Prog Brain Res* 144:47–60.
28. Raudies F, Brandon MP, Chapman GW, Hasselmo ME (2015) Head direction is coded more strongly than movement direction in a population of entorhinal neurons. *Brain Res* 1621:355–367.
29. Chelazzi L, Rossi F, Tempia F, Ghirardi M, Strata P (1989) Saccadic eye movements and gaze holding in the head-restrained pigmented rat. *Eur J Neurosci* 1(6):639–646.
30. de Araujo IET, Rolls ET, Stringer SM (2001) A view model which accounts for the spatial fields of hippocampal primate spatial view cells and rat place cells. *Hippocampus* 11(6): 699–706.
31. Wallace DJ, et al. (2013) Rats maintain an overhead binocular field at the expense of constant fusion. *Nature* 498(7452):65–69.
32. Huber G, et al. (2010) Novel rodent models for macular research. *PLoS One* 5(10): e13403.
33. Mizumori SJ, Williams JD (1993) Directionally selective mnemonic properties of neurons in the lateral dorsal nucleus of the thalamus of rats. *J Neurosci* 13(9):4015–4028.
34. Mizumori SJ, Miya DY, Ward KE (1994) Reversible inactivation of the lateral dorsal thalamus disrupts hippocampal place representation and impairs spatial learning. *Brain Res* 644(1):168–174.
35. Dale A, Cullen KE (2013) The nucleus prepositus predominantly outputs eye movement-related information during passive and active self-motion. *J Neurophysiol* 109(7):1900–1911.
36. Jacobs J, et al. (2013) Direct recordings of grid-like neuronal activity in human spatial navigation. *Nat Neurosci* 16(9):1188–1190.
37. Canto CB, Wouterlood FG, Witter MP (2008) What does the anatomical organization of the entorhinal cortex tell us? *Neural Plast* 2008:381243.
38. Suzuki WA, Miller EK, Desimone R (1997) Object and place memory in the macaque entorhinal cortex. *J Neurophysiol* 78(2):1062–1081.
39. Kim S, Sapiurka M, Clark RE, Squire LR (2013) Contrasting effects on path integration after hippocampal damage in humans and rats. *Proc Natl Acad Sci USA* 110(12): 4732–4737.
40. Moser EI, Kropff E, Moser M-B (2008) Place cells, grid cells, and the brain's spatial representation system. *Annu Rev Neurosci* 31:69–89.
41. Moser EI, et al. (2014) Grid cells and cortical representation. *Nat Rev Neurosci* 15(7): 466–481.
42. Jutras MJ, Fries P, Buffalo EA (2009) Gamma-band synchronization in the macaque hippocampus and memory formation. *J Neurosci* 29(40):12521–12531.
43. Jutras MJ, Fries P, Buffalo EA (2013) Oscillatory activity in the monkey hippocampus during visual exploration and memory formation. *Proc Natl Acad Sci USA* 110(32): 13144–13149.
44. Berens P (2009) CircStat : A MATLAB Toolbox for Circular Statistics. *J Stat Softw* 31(1): 128–129.
45. Saleem KS, Logothetis NK (2007) *A Combined MRI and Histology Atlas of the Rhesus Monkey Brain in Stereotaxic Coordinates* (Academic, London).
46. Pettersen KH, Devor A, Ulbert I, Dale AM, Einevoll GT (2006) Current-source density estimation based on inversion of electrostatic forward solution: Effects of finite extent of neuronal activity and conductivity discontinuities. *J Neurosci Methods* 154(1-2):116–133.
47. Zar JH (2010) *Biostatistical Analysis* (Prentice-Hall/Pearson, Upper Saddle River, NJ), 5th Ed.
48. Skaggs WE, Mcnaughton BL, Gothard KM, Markus EJ (1993) An information-theoretic approach to deciphering the hippocampal code. *Adv Neural Inf Process Syst* 5: 1030–1037.
49. Maris E, Oostenveld R (2007) Nonparametric statistical testing of EEG- and MEG-data. *J Neurosci Methods* 164(1):177–190.
50. Langston RF, et al. (2010) Development of the spatial representation system in the rat. *Science* 328(5985):1576–1580.
51. Solstad T, et al. (2008) Representation of geometric borders in the entorhinal cortex. *Science* 322(5909):1865–1868.
52. Itti L, Koch C, Niebur E (1998) A model of saliency-based visual attention for rapid scene analysis. *IEEE Trans Pattern Anal Mach Intell* 20(11):1254–1259.